*International Journal for Modern Trends in Science and Technology*
*Volume 10, Issue 05*, pages 92-100.
ISSN: 2455-3778 online
Available online at: http://www.ijmtst.com/vol10issue05.html
DOI: https://doi.org/10.46501/IJMTST1005014

# Developing a Single-Stage, High-Efficiency Control Strategy with Integrated Energy Management for Photovoltaic/Battery Hybrid Systems

**Narendra Babu Kattepogu[1], Thati Venkata M. Lakshmi[1] , Marumudi Bhargav[2],Patan Javed Khan[2], Inavolu Kiranmai[2], Renumanugu Lakshman[2]**

[1]Assistant Professor, Department of Electrical and Electronics Engineering, SRK Institute of Technology-Enikepadu, Vijayawada-521108, Andhra Pradesh, India
[2]Department of Electrical and Electronics Engineering, SRK Institute of Technology-Enikepadu, Vijayawada-521108, Andhra Pradesh, India

**To Cite this Article**
Narendra Babu Kattepogu, Thati Venkata M. Lakshmi , Marumudi Bhargav, Patan Javed Khan, Inavolu Kiranmai and Renumanugu Lakshman, Developing a Single-Stage, High-Efficiency Control Strategy with Integrated Energy Management for Photovoltaic/Battery Hybrid Systems, International Journal for Modern Trends in Science and Technology, 2024, 10(05), pages. 92-100. https://doi.org/10.46501/IJMTST1005014

**Article Info**
Received: 22 April 2024; Accepted: 13 May 2024; Published: 15 May 2024.



## ABSTRACT

***Proportional–integral (PI) energy strategy (EMS) and microgrid operations are proposed to work independently of the grid in this research paper. the photovoltaic system It delivers exactly what is needed. It uses DC/DC and DC/AC converters in addition to power tracking to maximise the PV energy. Classical PI control involves controlling parameters like state of charge (SOC). The three different scenarios are to take the maximum power-point tracking (MPPT) benefit into account for power distribution and battery charging/discharging. The Matlab/Simulink simulation shows the performance of the proposed power generation system in various operating conditions, with the corresponding control algorithms enabled.***

***Keywords— DC microgrid; energy management; hybrid power system; energy efficiency, Induction motor drive, EV Application***

## 1.INTRODUCTION

In power grids, the microgrid is defined as the distributed energy system (IDES), which includes energy storage like batteries and supercapacitors to balance generated power and consumed power. Together and separate for small areas, all of these items are used as a single grid [6,7]. Generally, microgrids are considered a collection of grids as shown in Figure 1. using a utility grid for power distribution has some drawbacks, such as loss of electricity in transmission, air pollution from the generation phases, and global warming due to conventional sources Microgrids offers a solution to these issues. Microgrids can lessen the loss, reduce CO2 emissions, especially when using renewable energy for power generation. There are a few advantages, too, such as reducing the risk of outages, selling power to national grids or net metering. besides storage elements, the overall system efficiency is maximised when using

renewable power sources [9–11] An energy management system (EM) controls the microgrid (MGR). it employs many techniques to improve performance These control methods include a PID control, a classic proportional integral (PI) control, and an equivalent decoupling (EMC)

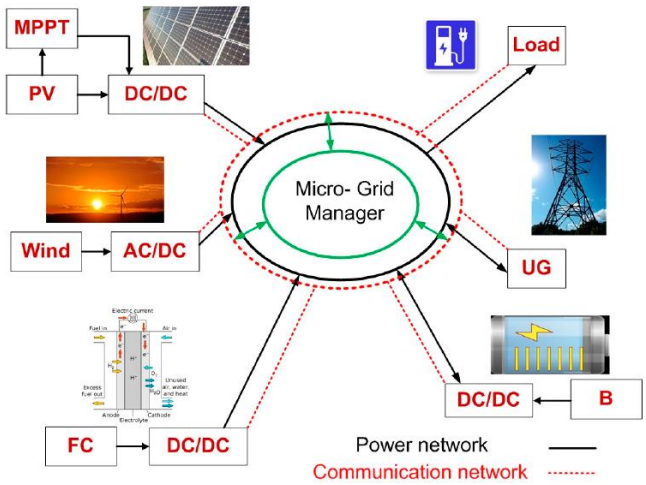


**Figure 1.** Configuration of DC microgrid

Alternative current microgrid (ACMG) and direct current microgrid (DCMG) were discussed by Manoj et al. [13]. (DCMG). The DCMG has some advantages over the ACMG, such as higher e ciency, easier DC bus communication, and device reliabilities. They confirmed that power disturbance is influenced by three factors in DCMGs: power exchange fluctuation, power variance between the storage system and the power sources, and quick changes in the DC bus load.

Ravichandrudu et al. [14] developed a renewable-energy-based MG system that has the advantages of using renewable energy sources and reducing transmission losses by using wind and hydro.

## 2. MODEL OF PV CELL

When light is shined on the solar cell, it will generate voltage. They are shown in the Fig1

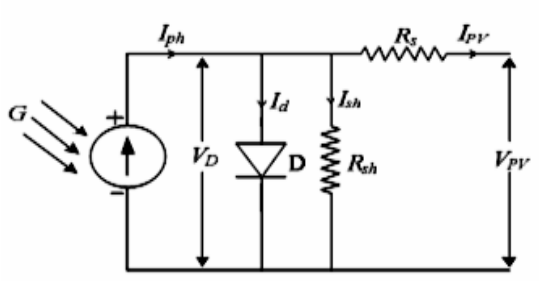


Fig1:mathematical model of PV cell

PV panel is modelled using mathematical equations (1)-(6) as given below

The current from PV panel is given by

$$I_{pv} = I_{ph} - I_d - I_{sh}$$

Where $I_{pv}$ = Current from PV panel

$I_{ph}$ = Photo generated Current

$I_d$ = Diode current

$I_{sh}$ =Shunt current

The Photo generated current is given by

$$Iph = G \times (Isc + (K_i \times (T_{op} - T_{ref}))) \quad (2)$$

Where G = Irradiation (w/m²)

$I_{sc}$ = Short circuit Current

$K_i$ = Temp.Coefficient of $I_{sc}$ ($2.2*10^{-23}$)

$T_{op}$ = Operating Temperature in $^0$C

$T_{ref}$ = Reference Temperature (25 $^0$C)

The diode current is given by

$$I_d = I_s \times (e^{q\times(\frac{V_{pv}+I_{pv}\times Rs}{Ns\times n\times V_t\times c})} - 1) \quad (3)$$

Where Is = Saturation Current

$V_{pv}$ = PV Panel output voltage

$R_s$ = Series resistance (0.01 Ω)

$V_t$ = Thermal Voltage = $\left(\frac{K*Top}{q}\right)$

n = Ideality Factor (1-2)

C = Total no. of Cells

$N_s$ = No. of cells in series

Q = Charge of an electron = $1.602*10^{-19}$ C

K = Boltzmann Constant = $1.38*10^{-23}$

The saturation current is given by

$$I_s = I_{rs} \times \left(\frac{T_{op}}{T_{ref}}\right) \times e^{\left(\frac{1}{T_{op}} - \frac{1}{T_{ref}}\right)\times\left(\frac{E_g\times q}{K\times n}\right)} \quad (4)$$

Where the reverse saturation current is given by

$$I_{rs} = \frac{I_{sc}}{e^{\left(\frac{q\times V_{oc}}{K\times C\times T_{op}\times n}\right)} - 1} \quad (5)$$

Where $E_g$ = Energy Gap of PV material =1.12ev

The shunt current is given by

$$I_{sh} = \left(\frac{V_{pv} + (I_{pv}\times R_s)}{R_{sh}}\right) \quad (6)$$

The number of cells to be connected to form an array is considered by taking a practical PV Panel electrical data Table 1.The I-V and P-V characteristics of the modeled PV panel conform to the manufacturer data.

## 3. ENERGY MANAGEMENT SYSTEM IN DC MICROGRID

In the following figure, the PV/battery distributed system is shown. This is a three-port device connecting a PV and a DCload. It serves as a buffer, which means it can be charged or discharged to ensure equalise the battery power output. as shown in Fig. 2,the power-density system utilises the integrated topology to do the DC-to-to-V and V-to-B buck/boost converters.

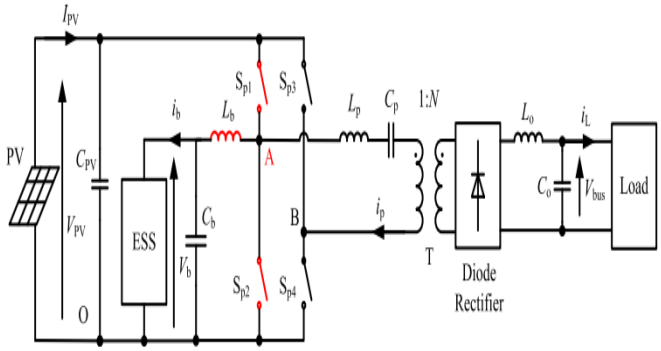


FIGURE 3.2. The proposed PV/battery hybrid distributed power generation system.

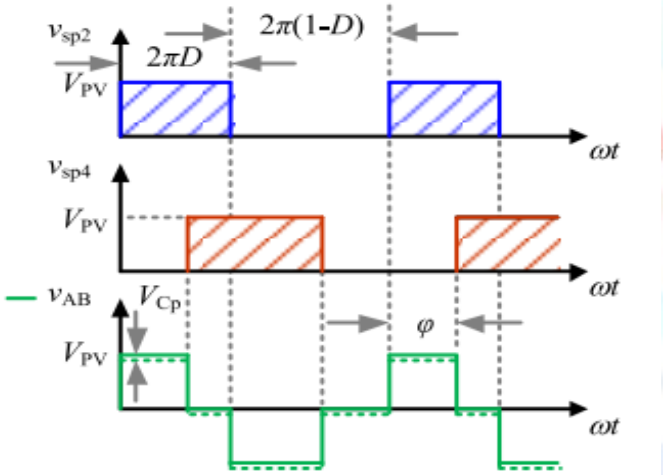


FIGURE 3.3. Modulation strategy of the full bridge with the phase shiftangle' and the duty cycle D.

This bridge utilises a modified phase shift modulation, as shown in Fig. 3. the two switching leg-to-limbs of the primary bridge are offset In addition, the duty cycle of switch A on the right leg 1 can be decreased, while the other cycles at 50 percent

Here, the primary side of the HF transformer's bidirectionalium-boost converter is highlighted in Fig. 2 Bidirectional topology makes the leg A battery and capacitor redundant. when the battery is charged to positive Ib, the topology isin When the voltage is reduced to IB< 0, the topology remains active Thus, two-way power is available for the battery charging/discharging can be applied The proposed control flowchart in Fig. 3.4 is outlined

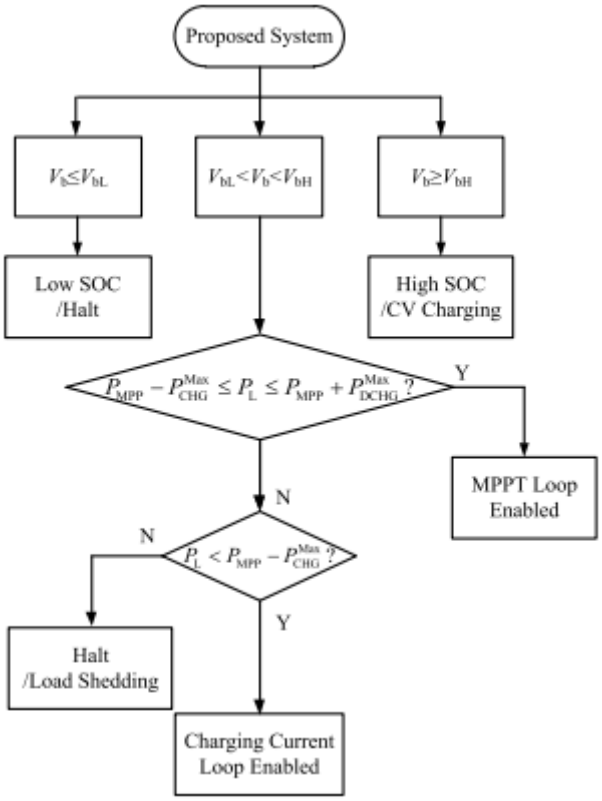


FIGURE 3.4.Flow diagram of the proposed control algorithm.

## 4. PROPOSED THREE PORT CONVERTER FED INDUCTION MOTOR

The three-phase machine is the most widely used machine in industry. A motor is almost always used for induction because it is the inadvevise choice. By itself, single-phase induction motors are quite common in consumer purposes.

It can be obtained using either the stator voltage control or the rotor resistance variation. However, they result in poor efficiency at low speeds The most effective speed control method is to vary the supply frequency. As a result, this results in wide spectrum of speed.

As long as the machine is not running at full speed, the ratio v/f remains constant. This keeps the engine's horsepower/torque output at a constant. However, torque drops off at lower frequencies and this has to be made up for by applying higher voltage.

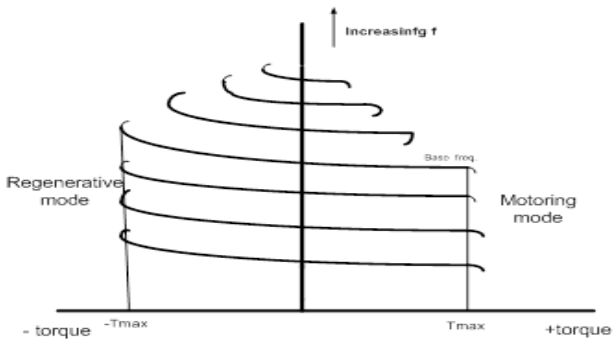


Fig.4.3 (a). Speed Torque Characteristics of Induction Motor with frequency variation

The above curve suggests that the speed control and braking operation are available from nearly zero speed to above synchronous speed.

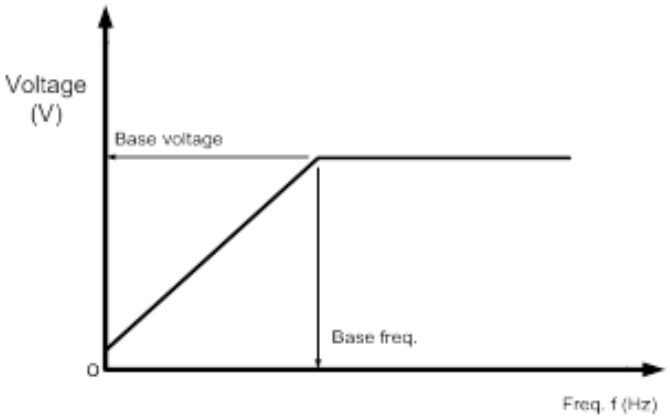


Fig.4.3 (b).voltage and frequency variation in VSI fed Induction motor

It can be shown in Fig.4.3 (b) that V is held constant above base speed while freq. increases. Because of the following characteristics, variable frequency control provides good running and transient performance:

(a) From zero to above base speed, speed control and braking are possible.

(b) The operation can be carried out at full torque with reduced current during transients (starting, braking, and speed reversal), resulting in good dynamic response.

(c) Copper losses are minimised, and efficiency and power factor are high since the operation is performed at all frequencies between synch. speed and maximum torque.

(d) The speed drop from no load to full load is minimal.

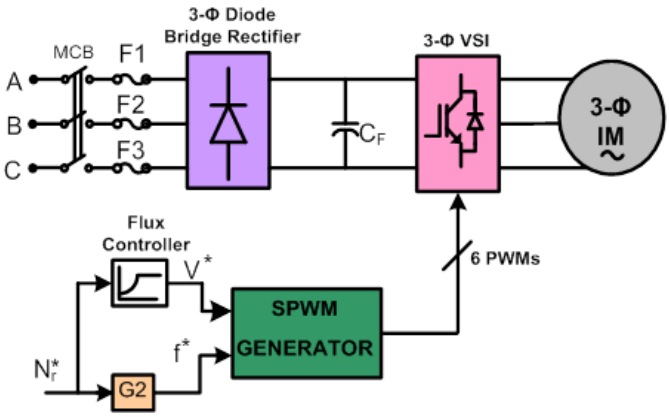


Fig:4.3 (c). Block Diagram Schematic of V/f control of VSI fed 3-phase Induction Motor drive

The block diagram of a V/f regulation of a VSI fed three phase induction motor drive is shown in Fig.4.3 (c). The reference frequency (f*) and reference voltage (V*) commands are determined according to the reference speed input command (Nr*) so that the V/f ratio remains constant. The SPWM generator receives the reference commands V* and f*, which produce 6-PWM pulses for the three-phase voltage source inverter, which drives the three-phase induction motor.

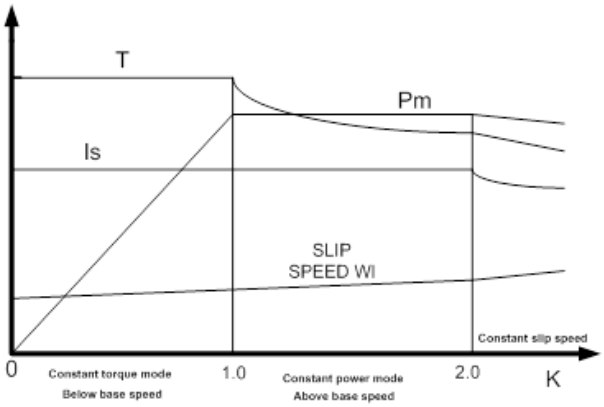


Fig.4.3(d). Modes of operation and variation of is, ωsl,, T and Pm with per unit frequency

## 5. SIMULATION RESULTS

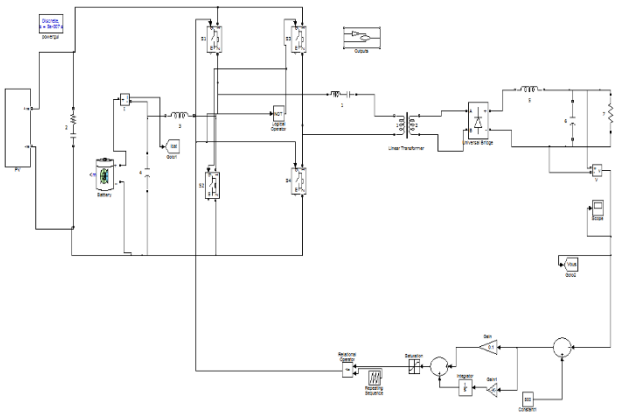

Fig 5.1 Diagram of Proposed System

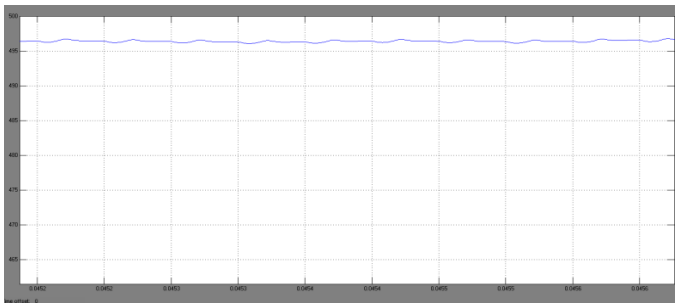

(a) DC bus voltage V bus;

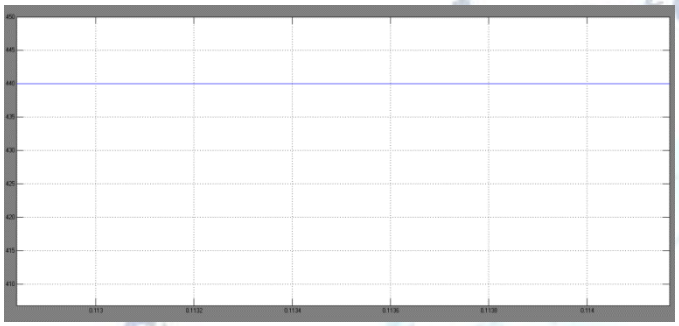

(b) PV voltage VPV;

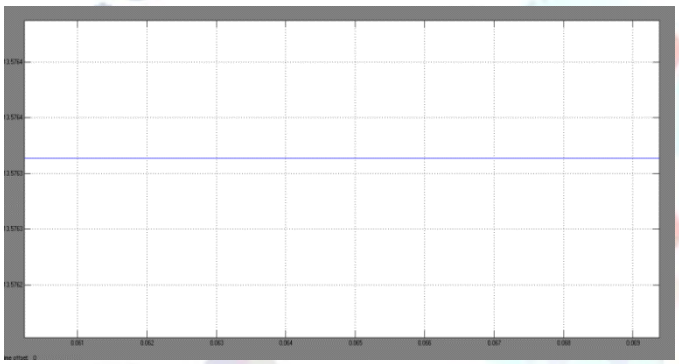

(c) PV current IPV;

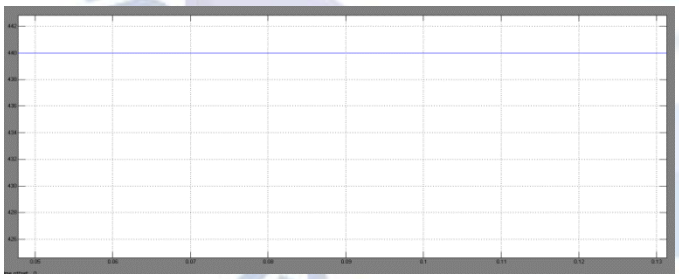

(d) PV reference voltage Vref;

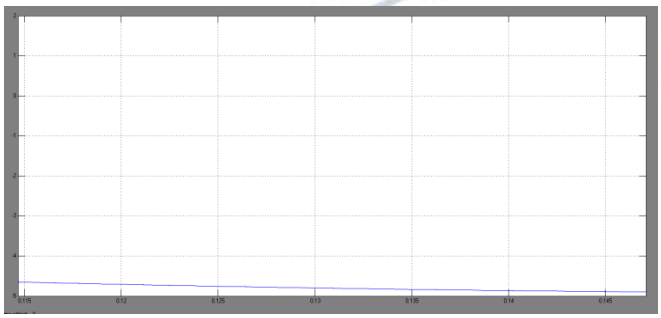

FIGURE 5.2 Steady state simulation results of operation scenario 2. (a) DCbus voltage Vbus; (b) PV voltage VPV; (c) PV current IPV; (d) PV reference voltage Vref; (e) Batter charging current ib.

Figure 5.2 depicts the operation's steady-state simulation performance. The following are the simulation conditions: The load power PL D 10 kW is based on a 1000 W/m2 irradiance and a temperature of 25°C. The DC bus voltage Vbus is regulated at the current value Vbus D 500 V, which is shown in Fig. 5.2, by controlling the phase shiftangle ' via a PI controller (a). Since the MPPT loop is activated in this scenario, the PV operates at full capacity, with VPV controlled near the ideal value VMPP D 435 V and IPV controlled near the ideal valueIMPP D 22 A, as shown in Fig. 5.2 (b), 5.2 (c), and 5.2 (d). The battery, as shown in Fig. 5.2(e), is in the discharging mode and supplies a portion of the load capacity.

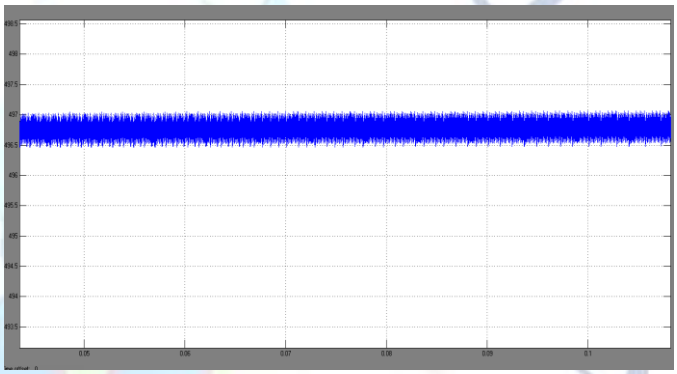

(a) DC bus voltage V bus;

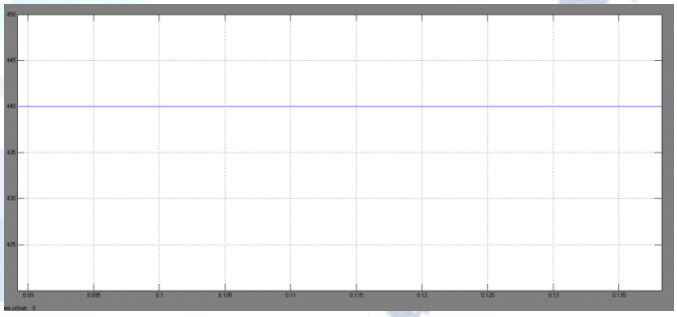

(b) PV voltage VPV;

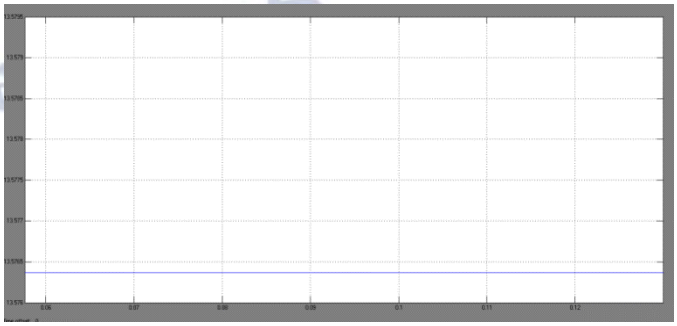

(c) PV current IPV;

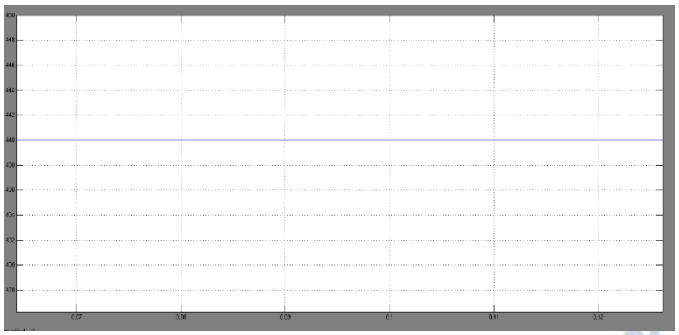

(d) PV reference voltage Vref;

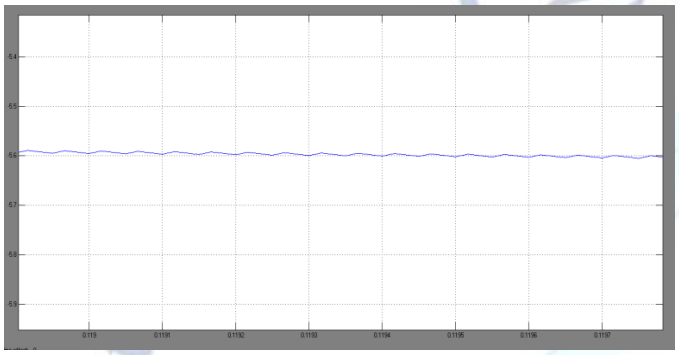

(e) Battery charging current ib.

FIGURE 5.3. Steady state simulation results of operation scenario 4. (a) DCbus voltage Vbus; (b) PV voltage VPV; (c) PV current IPV; (d) PV referencevoltage Vref; (e) Battery charging current ib.

Figure 5.3 illustrates the operation's steady-state simulation performance. The following are the simulation conditions: The load power PL D 8 kW is based on a 1000 W/m2 irradiance and a temperature of 25°C. As shown in Fig. 5.3, the DC bus voltage Vbus is operated at the current value Vbus D 500 V. (a). The MPPT loop is also allowed in this case, as shown in Fig. 5.3 (b), 5.3 (c), and 5.3 (d), and the PV operates at the highest power point, with VPV controlled near the ideal value VMPP D 435 V and IPV controlled near the ideal valueIMPP D 22 A. In this case, the battery works in the charging mode, and the excess power from the PV can be retained in the battery, as shown in Fig. 5.3 (e).

.

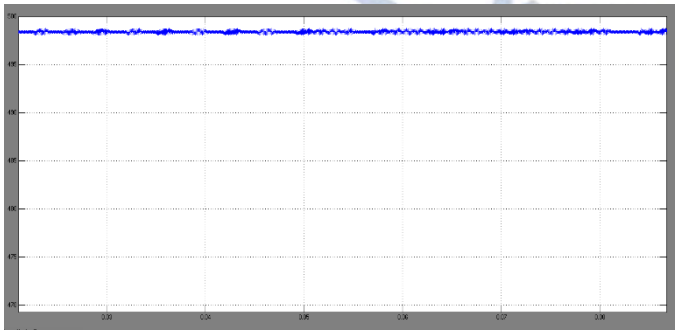

(a)

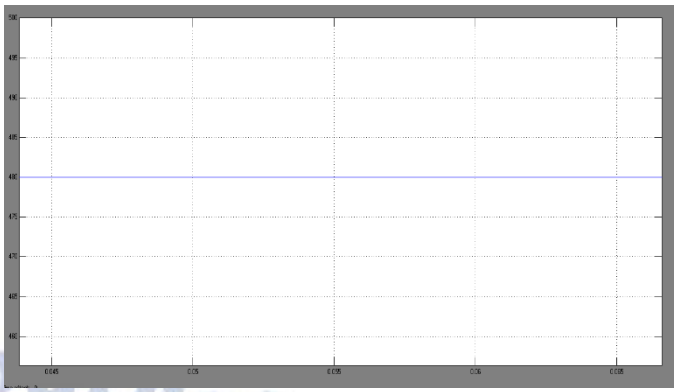

(b)

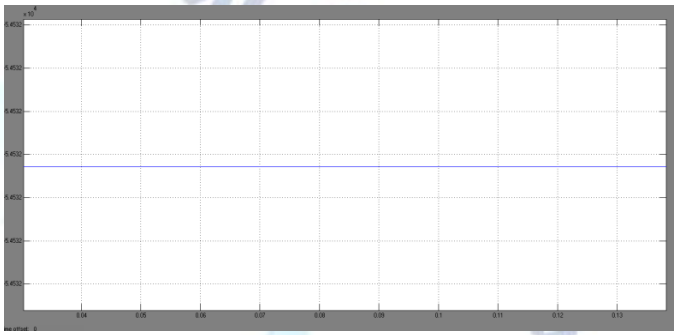

(c)

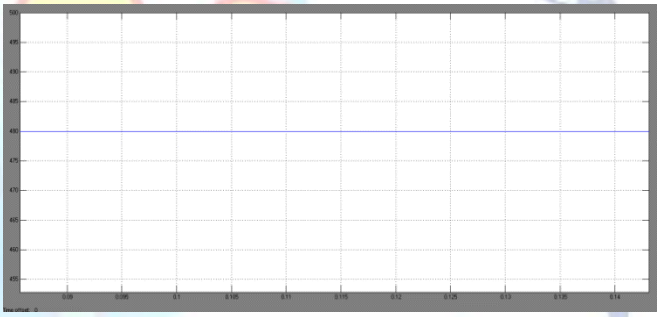

(d)

FIGURE 5.4 Steady state simulation results of operation scenario 5. (a) DCbus voltage Vbus; (b) PV voltage VPV; (c) PV current IPV; (d) Batterycharging current ib

The steady state results of the operation are shown in Fig. 5. Simulation is asfollows: The irradiance at 1000 W/m², the temperature of 25 C It is equal to the value in Fig. 4 as shown in Figure 5 (a). In this scenario, the maximum charge current I is set to 30A, and the MPPT charger is set to 0, which is illustrated in Fig. 5 (d). From Fig. 5.4 (b) and Fig. 5.4 (c), the PV would not be operating at the maximum power in this case.

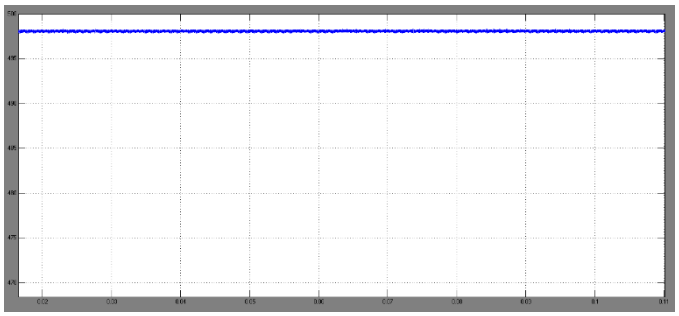

(a)

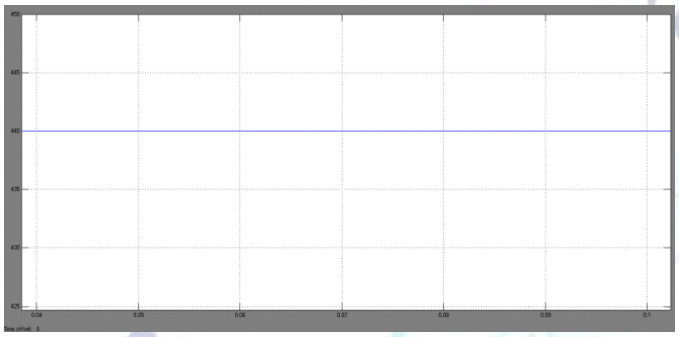

(b)

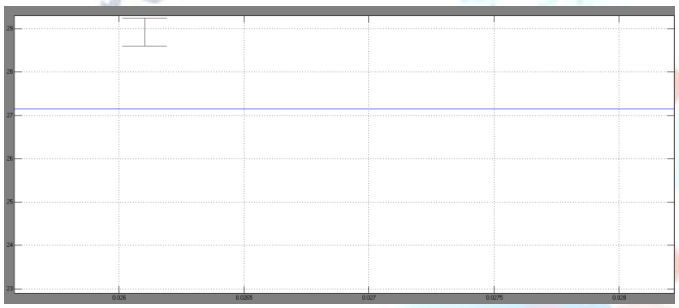

(c)

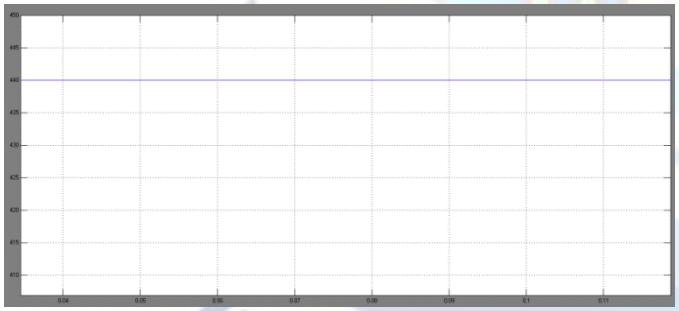

(d)

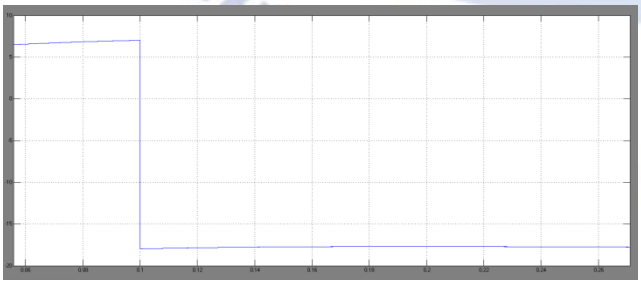

(e)

FIGURE 5.4. Simulation results with irradiance dropping from 1000 W/m2to 500 W/m2 at t D 2 s. (a) DC bus voltage Vbus; (b) PV voltage VPV; (c) PV current IPV; (d) PV reference voltage Vref; (e) Battery charging current ib.

The dynamic performance shown in Fig. 5, where irradiance decreases from 1000 W/m2 to 500 W/m2 at time "t" Other simulation rules are: Temperature: 25 C, the load: 8 kW during the voltage transition to bus 5 as shown in Fig. 5 (a). When in this situation, the MPPT always controls the duty cycle the PV voltage rises from Fig. 5. 4.4 (d) From Fig. 10 (b) and Fig. 10 (c), MPPT is accomplished with PV operating near its maximum power points From Fig. 10 (e), the irradiation incident can be considered to occur as a transition from scenario 4 to scenario 2, because the battery is first in charge and then after use.

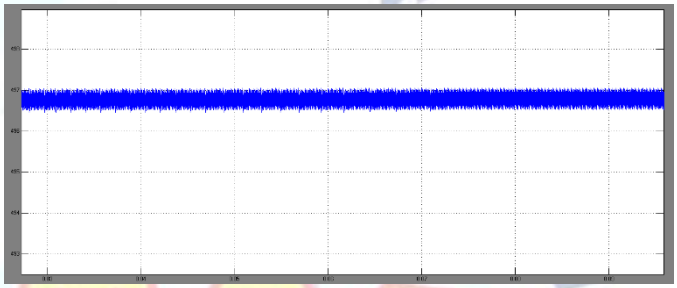

(a)

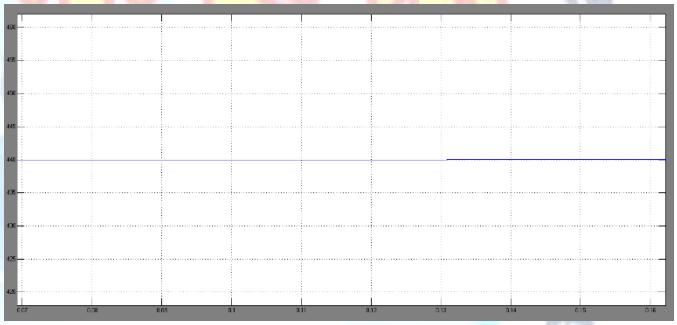

(b)

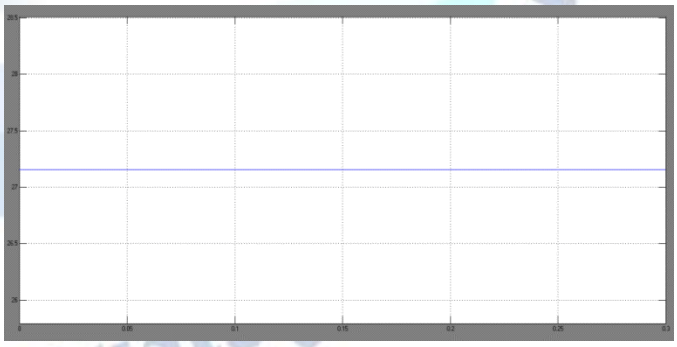

(c)

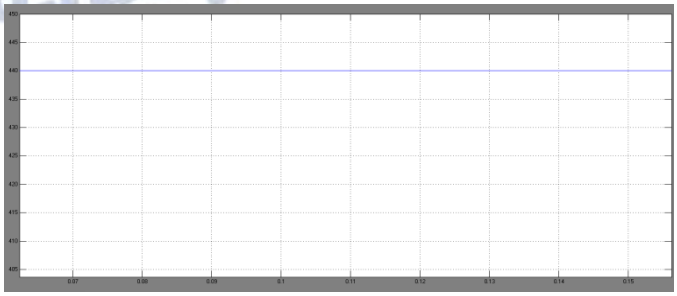

(d)

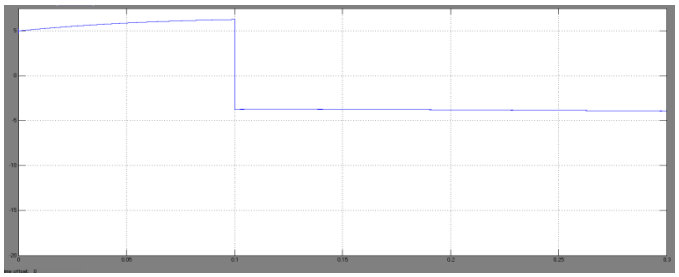

(e)

FIGURE 5.5. Simulation results with load power rising from 8 kW to 10 kWat t D 2 s. (a) DC bus voltage Vbus; (b) PV voltage VPV; (c) PV current IPV;(d) PV reference voltage Vref; (e) Battery charging current ib.

The dynamic system output power from 8 kW to 10 kW at time D 2 is shown in Figure 5. Other simulation rules are: (Virradiance 1000 W/m2, Temperature 25°C) In Fig. 5, the DC bus voltage does not fluctuate (a). Fig. 5 shortens from Fig. 5. b to Fig. 5 (d). This can be thought of as the result of the load rising from Scenario 5 to Scenario 2 in Figure 5 (e).

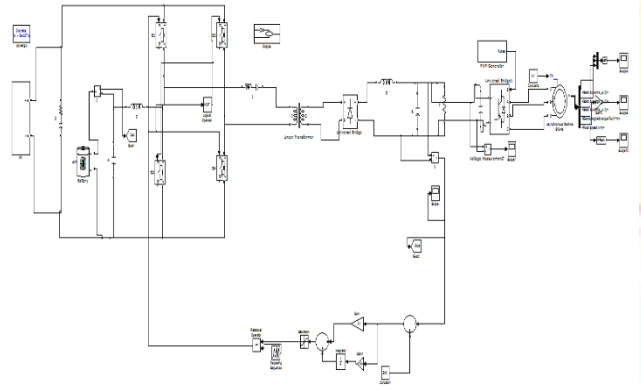

Fig 5.6 Simulink diagram of Proposed System power converter with Induction Motor drive

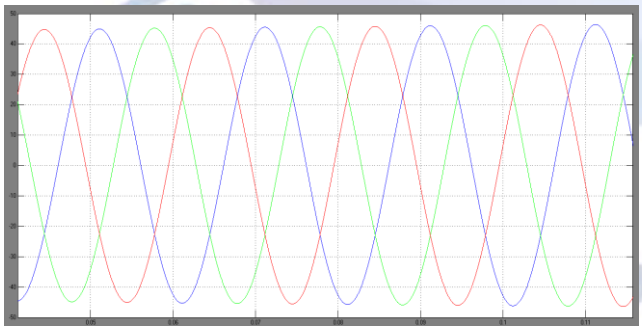

Fig 5.7 Simulation waveforms of Induction motor drive stator current characteristics

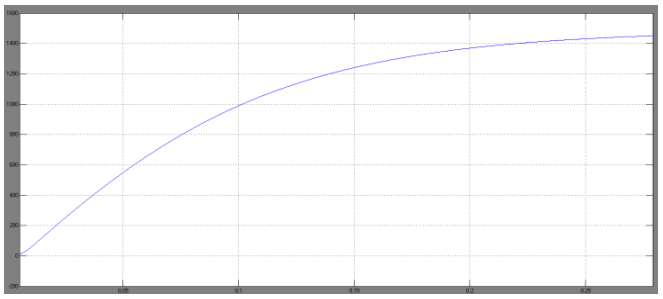

Fig 5.8 Simulation waveforms of Induction motor drive speed characteristics

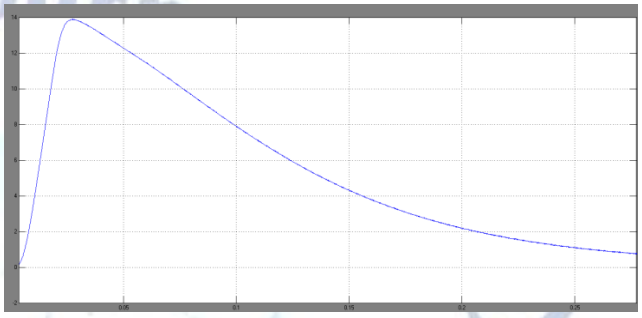

Fig 5.9 Simulation waveforms of Induction motor drive Torque characteristics

## 6. Conclusion

Using a microgrid with a renewable hybrid would be a wonderful, efficient, and clean power solution. It's able to replace conventional fuel. Here, the three-port converter has been integrated into the PV/battery hybrid power generation system. It solves the source's problems and provides adequate power for the load. Because of cloud cover and night time, the PV array will provide the main power for the system. The proposed system has attributes include higher power density and/reliability. The full bridge and switch cycle phase shift angles are used to obtain the required DC bus voltage, which helps realise power balance among three ports. One way or another, many operating scenarios are examined, along with a comprehensive energy management and control strategy is proposed. You can choose to use the priority controller to allow only one of the control loops to optimise the system performance; it takes battery charging and performance into consideration.

### Conflict of interest statement

Authors declare that they do not have any conflict of interest.

## References


[1] F. Blaabjerg, Z. Chen, and S. B. Kjaer, ‘‘Power electronics as efficientinterface in dispersed power generation systems,’’ IEEE Trans. PowerElectron., vol. 19, no. 5, pp. 1184–1194, Sep. 2004.

[2] J. M. Carrasco, L. G. Franquelo, J. T. Bialasiewicz, E. Galvan, R. Potillo,M. M. Prats, J. I. Leon, and N. Moreno-Alfonso, ''Power-electronic systems for the grid integration of renewable energy sources: A survey,'' IEEETrans. Ind. Electron., vol. 53, no. 4, pp. 1002–1016, Jun. 2006.

[3] BP Statistical Review of World Energy, British Petroleum, London, U.K.,Jun. 2018.

[4] J. P. Barton and D. G. Infield, ''Energy storage and its use with intermittent renewable energy,'' IEEE Trans. Energy Convers., vol. 19, no. 2,pp. 441–448, Jun. 2004.

[5] M. S. Whittingham, ''History, evolution, and future status of energy storage,'' Proc. IEEE, vol. 100, pp. 1518–1534, May 2012.

[6] C. A. Hill, M. C. Such, D. Chen, J. Gonzalez, and W. M. Grady, ''Batteryenergy storage for enabling integration of distributed solar power generation,'' IEEE Trans. Smart Grid, vol. 3, no. 2, pp. 850–857, Jun. 2012.

[7] Z. Yi, W. Dong, and A. H. Etemadi, ''A unified control and power management scheme for PV-battery-based hybrid microgrids for both gridconnected and islanded modes,'' IEEE Trans. Smart Grid, vol. 9, no. 6,pp. 5975–5985, Nov. 2018.

[8] H. Mahmood, D. Michaelson, and J. Jiang, ''Decentralized power management of a PV/battery hybrid unit in a droop-controlled islanded microgrid,''IEEE Trans. Power Electron., vol. 30, no. 12, pp. 7215–7229, Dec. 2015.

[9] K. Sun, L. Zhang, Y. Xing, and J. M. Guerrero, ''A distributed controlstrategy based on DC bus signaling for modular photovoltaic generation systems with battery energy storage,'' IEEE Trans. Power Electron.,vol. 26, no. 10, pp. 3032–3045, Oct. 2011.

[10] S. Adhikari and F. Li, ''Coordinated V-f and P-Q control of solar photovoltaic generators with MPPT and battery storage in microgrids,'' IEEETrans. Smart Grid, vol. 5, no. 3, pp. 1270–1281, May 2014.

[11] S. K. Kollimalla, M. K. Mishra, and N. L. Narasamma, ''Design and analysis of novel control strategy for battery and supercapacitor storage system,''IEEE Trans. Sustain. Energy, vol. 5, no. 4, pp. 1137–1144, Oct. 2014.

[12] S. Wen, S. Wang, G. Liu, and R. Liu, ''Energy management and coordinated control strategy of PV/HESS AC microgrid during Islanded operation,'' IEEE Access, vol. 7, pp. 4432–4441, 2019.

[13] W. Jiang and B. Fahimi, ''Multiport power electronic interface—Concept,modeling, and design,'' IEEE Trans. Power Electron., vol. 26, no. 7,pp. 1890–1900, Jul. 2011.

[14] H. Krishnaswami and N. Mohan, ''Three-port series-resonant DC–DCconverter to interface renewable energy sources with bidirectional loadand energy storage ports,'' IEEE Trans. Power Electron., vol. 24, no. 10,pp. 2289–2297, Oct. 2009.

[15] H. Tao, J. L. Duarte, and M. A. M. Hendrix, ''Three-port triple-half-bridgebidirectional converter with zero-voltage switching,'' IEEE Trans. PowerElectron., vol. 23, no. 2, pp. 782–792, Mar. 2008.

[16] Z. Qian, O. Abdel-Rahman, and I. Batarseh, ''An integrated four-portDC/DC converter for renewable energy applications,'' IEEE Trans. PowerElectron., vol. 25, no. 7, pp. 1877–1887, Jul. 2010.

[17] H. Al-Atrash and I. Batarseh, ''Boost-integrated phase-shift full-bridgeconverter for three-port interface,'' in Proc. IEEE Power Electron. Spec.Conf., Jun. 2007, pp. 2313–2321.

[18] W. Li, J. Xiao, Y. Zhao, and X. He, ''PWM plus phase angle shift (PPAS)control scheme for combined multiport DC/DC converters,'' IEEE Trans.Power Electron., vol. 27, no. 3, pp. 1479–1489, Mar. 2012.

[19] T. Esram and P. L. Chapman, ''Comparison of photovoltaic array maximumpower point tracking techniques,'' IEEE Trans. Energy Convers., vol. 22,no. 2, pp. 439–449, Jun. 2007.